Supporting Information

Why Does Dimethyl Carbonate Dissociate Li Salt Better Than Other Linear Carbonates?: Critical Role of Polar Conformers

Hyejin Lee,[†,∥] Sunwook Hwang,[†,∥] Minju Kim,[‡] Kyungwon Kwak,[‡] Jaeho Lee,[§] Young-Kyu Han,[§,*] and Hochun Lee[†,*]

[†]Department of Energy Science and Engineering, DGIST, Daegu 42988, Republic of Korea

[‡]Center for Molecular Spectroscopy and Dynamics, Institute for Basic Science (IBS) & Department of Chemistry, Korea University, Seoul, 02841, Republic of Korea

[§]Department of Energy and Materials Engineering, Dongguk University, Seoul 04620, Republic of Korea

*Corresponding author:

E-mail: ykenergy@dongguk.edu

E-mail: dukelee@dgist.ac.kr

Experimental section

Chemicals: Lithium salt $LiPF_6$ (99.99%, Panaxetec), LiFSI (99.99%, Panaxetec), $LiClO_4$ (99.99%, Panaxetec), NaFSI (99.99%, Panaxetec), and KFSI (99.99%, Panaxetec) were prepared. Battery grade dimethyl carbonate (DMC), ethylmethyl carbonate (EMC), and diethyl carbonate (DEC) were provided by Panaxetec.

Ionic conductivities were measured by Orion VSTAR52 with 013605MD probe at 25 °C (Measuring Range: 10 μS cm^{-1}–200mS cm^{-1}, Cell constant: 0.55 cm^{-1}). Viscosities were obtained at 25 °C by vibro-viscometer (SV-10A) which has measuring range from 0.3 to 10000 mPa s. The minimum sample amount is 10 mL and measurement accuracy is ±3%.

PFG-NMR: The NMR measurements were performed inside a standard 5 mm NMR tube in 0.3 mL non-deuterated solvent without field/frequency locking at 293±0.2 K. The smaller inner NMR tube was inserted to a standard NMR tube with $CdCl_3$ 0.15 mL. The spectra were recorded on a Bruker Avance III 400 (400.13 MHz) spectrometer. The gradient strength was calibrated using samples with literature known and laboratory known diffusion coefficients.

For each experiment, 2 dummy scans and 16 scans were used with a relaxation delay of 2 s. The length of the gradient pulse was optimized for every nucleus in each sample and was 4.0–6.0 ms for 1H-, 14.0–20.0 ms for 7Li- and 5.6–9.4 ms for 19F-DOSYs and a diffusion time of 50 ms was used for all experiments. Sinusoidal shapes were used for the gradients and a linear gradient ramp with 12 increments for 1H and 10 increments for 7Li and 19F between 5 and 95% of the maximum gradient strength was applied for the diffusion relevant gradients. For the homospoil gradients, 9.165 and 7.046 G cm^{-1} were applied for HS1 and HS2. The spectra were processed with the Bruker program Topspin® and the diffusion coefficients were calculated with the Bruker software T1/T2 package.

Raman measurements: The Raman spectra of the electrolyte solutions were recorded using a monochromator (Thermo Scientific, Nicolet almeca XR). Excitation was carried out with a 780 nm line from an argon ion laser. The electrolyte samples were contained in glass vials and measured using 180-degree beam path accessory. Each spectrum consisted of 64 accumulations averaged together and their resolution was 0.5 cm^{-1}.

DRS measurements: Dielectric relaxation was measured by Agilent 85070E Dielectric Probe Kit installed with N5247A PAN-X network analyzer. Dielectric relaxation spectroscopy (DRS) measures the interaction of an electrolyte with a time-dependent small-amplitude electric field. The dielectric spectra were recorded at 25°C in the frequency range $0.2 \leq \nu/\mathrm{GHz} \leq 20$. For an electrolyte solution of ion conductivity κ, DRS determines the dielectric constant, ε′(ν), and the total loss, η″(ν), which is related with the dielectric loss ε″(ν)

$$\eta''(\nu) = \varepsilon''(\nu) + \kappa/(2\pi\nu\varepsilon_o) \tag{1}$$

where ε_o is the permittivity of free space. The permittivity, ε′(ν), is the in-phase response of the sample to the electric field and the dielectric loss, ε″(ν), represents the out-of-phase response of the sample to the electric field. A typical example set of spectra is shown in supplementary information.

For the analysis of the DRS spectra, relaxation processes were fitted to the experimental **ε** by following a procedure described in the literature.[1] The best appropriate description of the experimental data is obtained with a superposition of Debye equations for the low frequency solute dispersion—solvent-shared ion pairs (SIPs) and contact ion pairs (CIPs)—and the high frequency solvent relaxation.

$$\varepsilon(\nu) = \frac{S_{SIPs}}{1 + i2\pi\nu\tau_{SIPs}} + \frac{S_{CIP}}{1 + i2\pi\nu\tau_{CIP}} + \frac{S_S}{1 + i2\pi\nu\tau_S} + \varepsilon_\infty \tag{2}$$

In Eq. (2), the amplitude of SIPs ($S_{SIPs} = \varepsilon - \varepsilon_{CIP}$), amplitude of CIP ($S_{CIP} = \varepsilon_{CIP} - \varepsilon_{s)}$, amplitude of solvent ($S_s = \varepsilon_s - \varepsilon_\infty$) and ε is the static permittivity, ε_∞ is the infinite-frequency limit, ε_{CIP} is

the dielectric constant of CIP, and ε_s stands for the dielectric constant of free solvent. Amplitude (S) value of relaxation processes arising from the reorientation of ion pair dipoles could be analyzed by the Cavell equation.[2,3] From the Cavell equation, it is confirmed that the amplitudes are proportional to the concentration of certain species.

Computational details: A computational study based on Kohn−Sham DFT was extensively performed. All of the molecular structures were optimized with no symmetry constraints using the B3LYP functional[4,5] and 6-311G(d,p) basis set implemented in the Gaussian09 software package.[6] The continuum solvation model SMD was used in the geometry optimization and in the harmonic frequency calculations for describing solvation effects. The solvent options of each carbonate molecule were DMC (dibutylether, $\varepsilon = 3.05$), EMC (tetralin, $\varepsilon = 2.77$), and DEC (dipropylamine, $\varepsilon = 2.91$) when describing pure LCs Raman spectroscopy. A dielectric constant of 11.0, corresponding to static permittivity of three solutions with 1M $LiPF_6$ in Figure 1f, was used for obtaining the reaction Gibbs free energies in Table 2. To confirm local minima, frequency calculations were carried out with the same functional and basis set as those used in the geometry optimization. All the DFT energy values consisted of zero-point energy (ZPE) correction and thermal corrections to evaluate Gibbs free energy were performed at 298.15 K and 1 atm. The DFT optimized structures are depicted in Figure S11–S13.

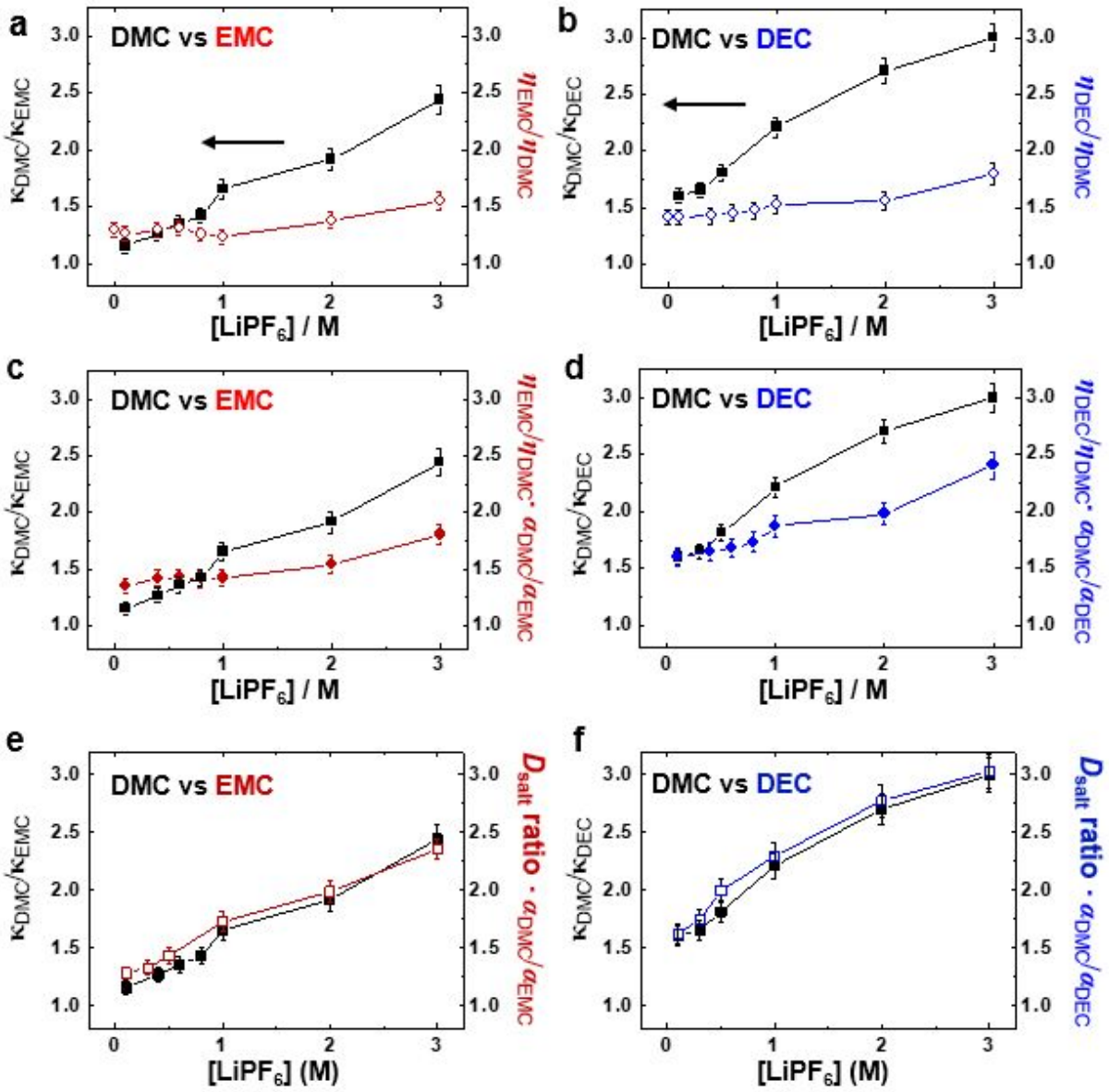

Figure S1. A comparison of ionic conductivity ratio (left y-axis, ■) and fluidity ratio (right y-axis, ○) of a) EMC and b) DEC to the DMC. The same comparison with product of fluidity and dissociation ratio (α, right y-axis, ●) of c) EMC and d) DEC to the DMC. α is a fraction of peak A concentration in Raman spectra of PF_6^- anion. Lastly, comparison of ionic conductivity ratio and product of D_{salt} ratio and α ratio (right y-axis, □) of e) EMC and f) DEC to the DMC as a function of salt concentration at 25 °C.

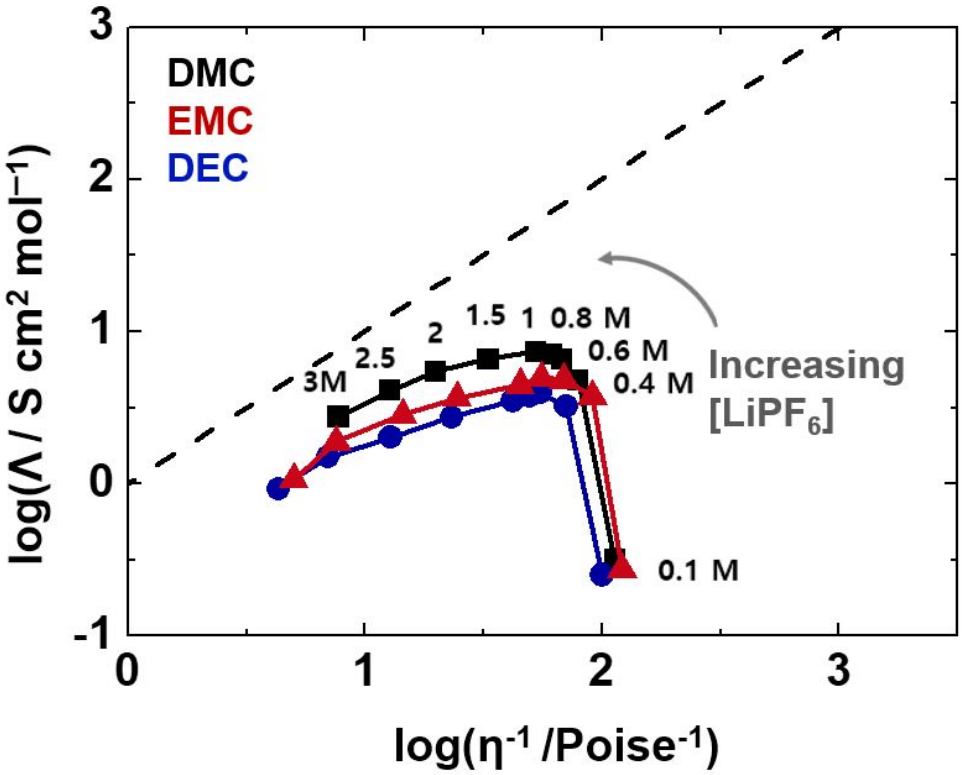

Figure S2. Walden plots of $LiPF_6$-DMC, $LiPF_6$-EMC, and $LiPF_6$-DEC as a function of salt concentration. Concentrations are indicated at each point.

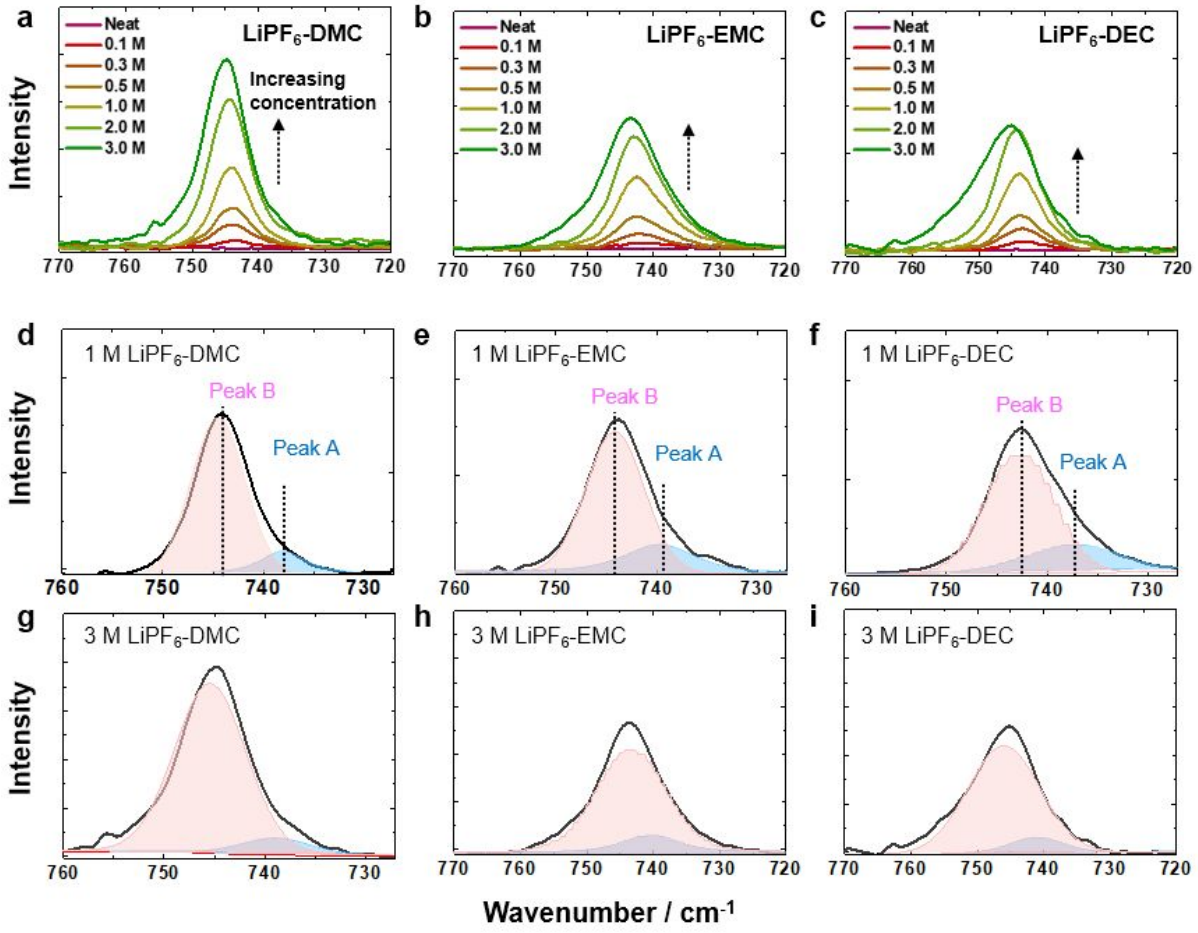

Figure S3. Raman spectra of PF_6^- anion in (a) $LiPF_6$-DMC, (b) $LiPF_6$-EMC, and (c) $LiPF_6$-DEC with changing salt concentration (0–3 M), increasing concentration from bottom to top. Peak positions are shifted to high waver number depending on salt concentration. (d-i) The fitted Raman spectra for PF_6^- anion of 1 M and 3 M electrolytes. The experimental spectra are denoted with black solid line, and peak A and peak B are assigned.

Derivation of D_{salt} and improved conductivity descriptors

We revisit the issue of the conductivity descriptors unexplained at the previous section (Figure S1). According to the Nernst-Planck relation, the ionic conductivity is determined both by the diffusivities and the population of mobile species.[7]

$$\kappa = \sum \frac{z_i^2 F^2}{RT} D_i c_i \tag{3}$$

$$D_i = \frac{k_B T}{6\pi\eta r_i} \tag{4}$$

where z_i, D_i, c_i, r_i, and η are the formal charge, diffusion coefficient, concentration, radius of the ionic species participating ionic conduction, and solution viscosity, respectively. Because the diffusivity involves both the contributions of the solution viscosity and the size of solvated species, the diffusivity should be more suitable parameter than the viscosity alone. Unfortunately, determining the accurate dimension and thus diffusivity of each ionic species, especially in concentrated solutions, is beyond the scope of this study. Instead, we simplified the issue by assuming that the salt-diffusion coefficient (D_{salt}) could represent the individual ionic mobility.

D_{salt} was estimated through the generalized Darken relation that correlates the binary diffusion coefficients (D_{0+}, D_{0-}, and D_{+-}) with the self-diffusion coefficients of Li ion, PF_6^- anion, and solvent (D_+, D_-, and D_0) as below.[8,9]

$$D_{0+} = \frac{x_0}{x_0 + x_+} D_+ + \frac{x_+}{x_0 + x_+} D_0$$

$$D_{0-} = \frac{x_0}{x_0 + x_-} D_- + \frac{x_-}{x_0 + x_-} D_0 \tag{5}$$

$$D_{+-} = \frac{x_-}{x_- + x_+} D_+ + \frac{x_+}{x_- + x_+} D_-$$

where x_i is the mole ratio of species i,

From the deduced binary diffusivities, D_{salt} can be obtained as follows.

$$D_{salt} = \frac{(z_+ - z_-)D_{0+}D_{0-}}{z_+ D_{0+} - z_- D_{0-}} \tag{6}$$

where z_i is the charge of species i ($z_+ = 1$ and $z_- = -1$ in this case). The deduced D_{salt} values in $LiPF_6$-DMC, EMC, and DEC solutions are presented in Figure S8.

Although several ideal conditions including no dynamic ion correlations ($D_{+-} \sim 0$), unit thermodynamic factor, and complete salt dissociation were assumed in deriving the D_{salt} values, the combined descriptor of the D_{salt} and salt-dissociation better explain the conductivity than the other descriptors (Figure S1e and f). Further detail on ionic conduction behavior including more accurate descriptor, the contribution of ion-hopping conduction, would require intricate sets of experiments and rigorous theoretical foundation based on concentration solution theory, which deserves future studies.

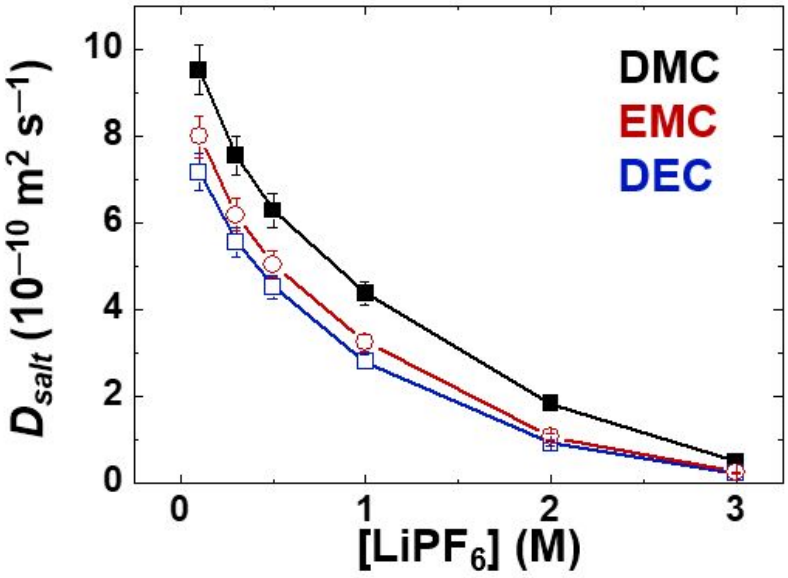

Figure S4. D_{salt} values of $LiPF_6$-DMC (black), EMC (red), and DEC (blue) solutions as a function of salt concentration at 25 °C.

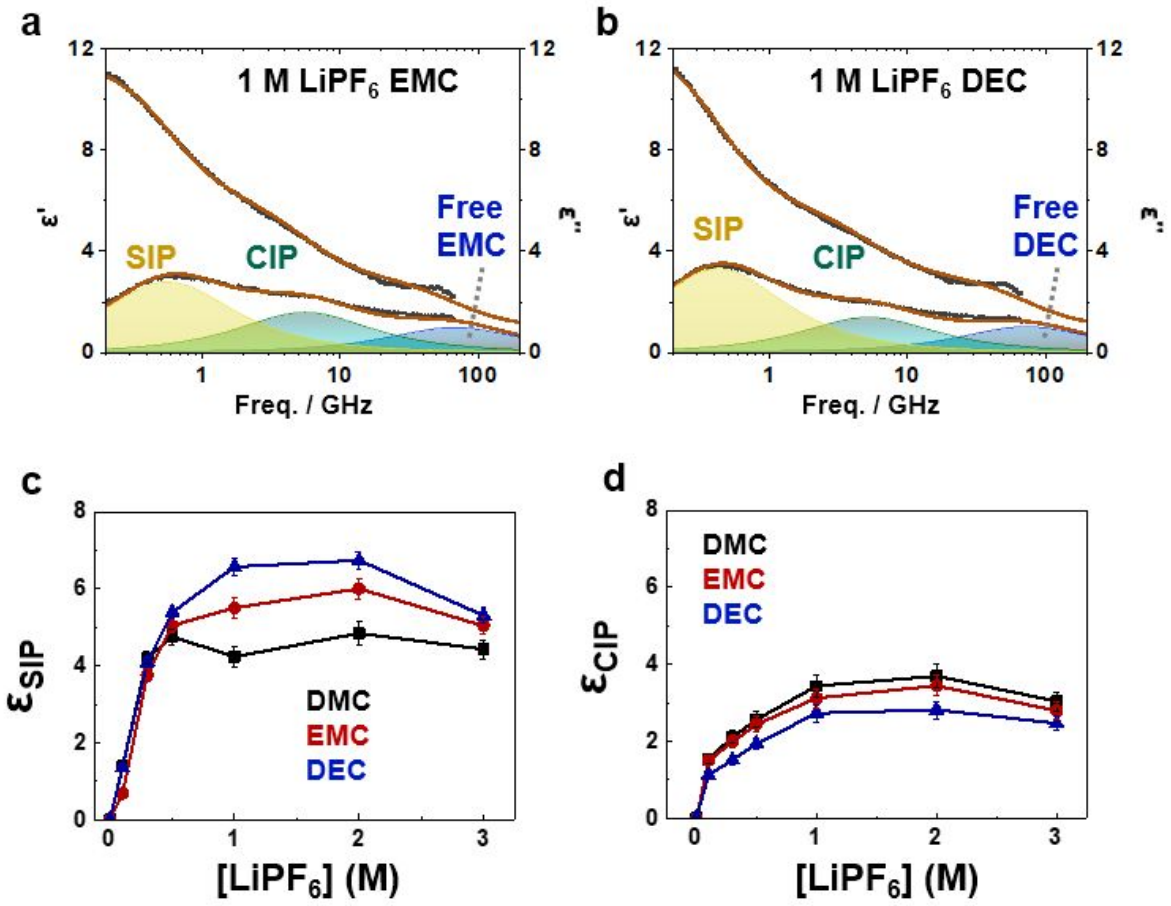

Figure S5. Representative DRS spectra and deconvoluted peaks of (a) 1 M $LiPF_6$-EMC and (b) 1 M $LiPF_6$-DEC. Relative permittivity, ε'(ν), dielectric loss, ε''(ν), with the spectrum calculated three Debye processes. The colored areas show the contributions of the SIPs, CIP and the solvent relaxation processes. Dielectric strength of (c) SIP and (d) CIP of $LiPF_6$-DMC, $LiPF_6$-EMC, and $LiPF_6$-DEC as a function of salt concentration.

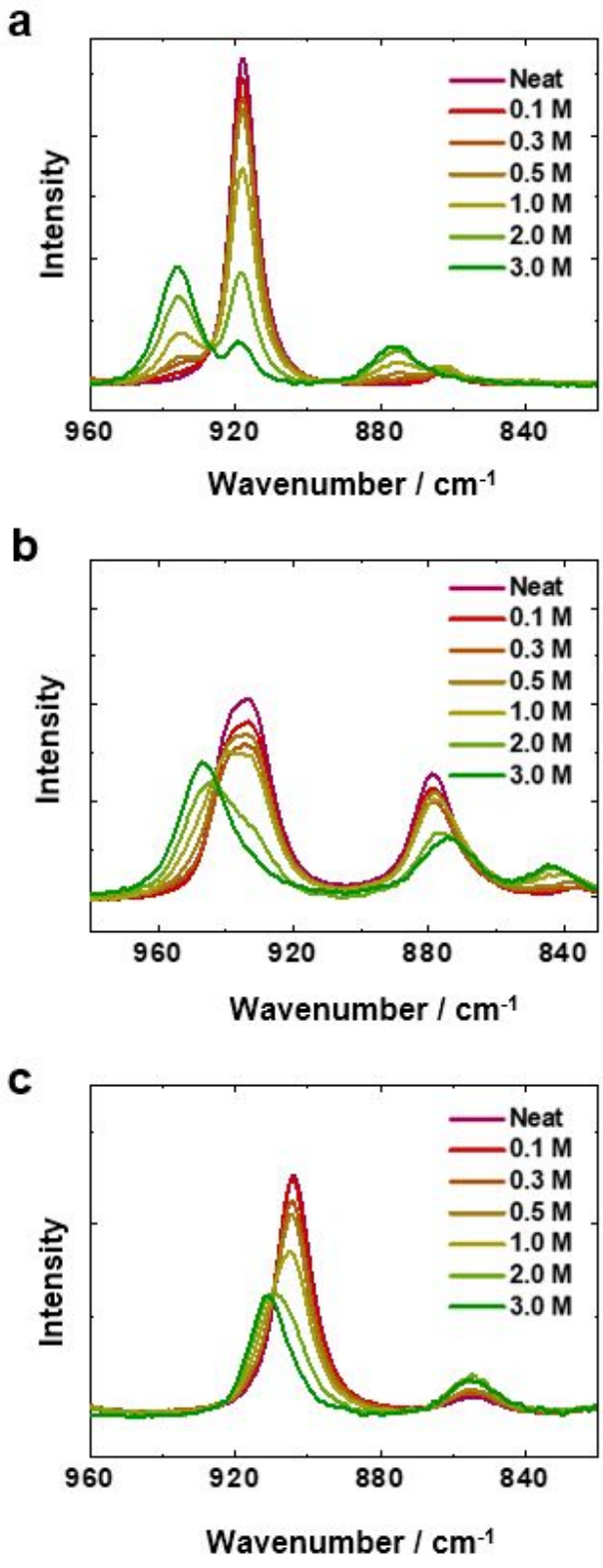

Figure S6. Raman spectra of (a) $LiPF_6$-DMC, (b) $LiPF_6$-DEC, and (c) $LiPF_6$-EMC with varying salt concentrations (0–3 M).

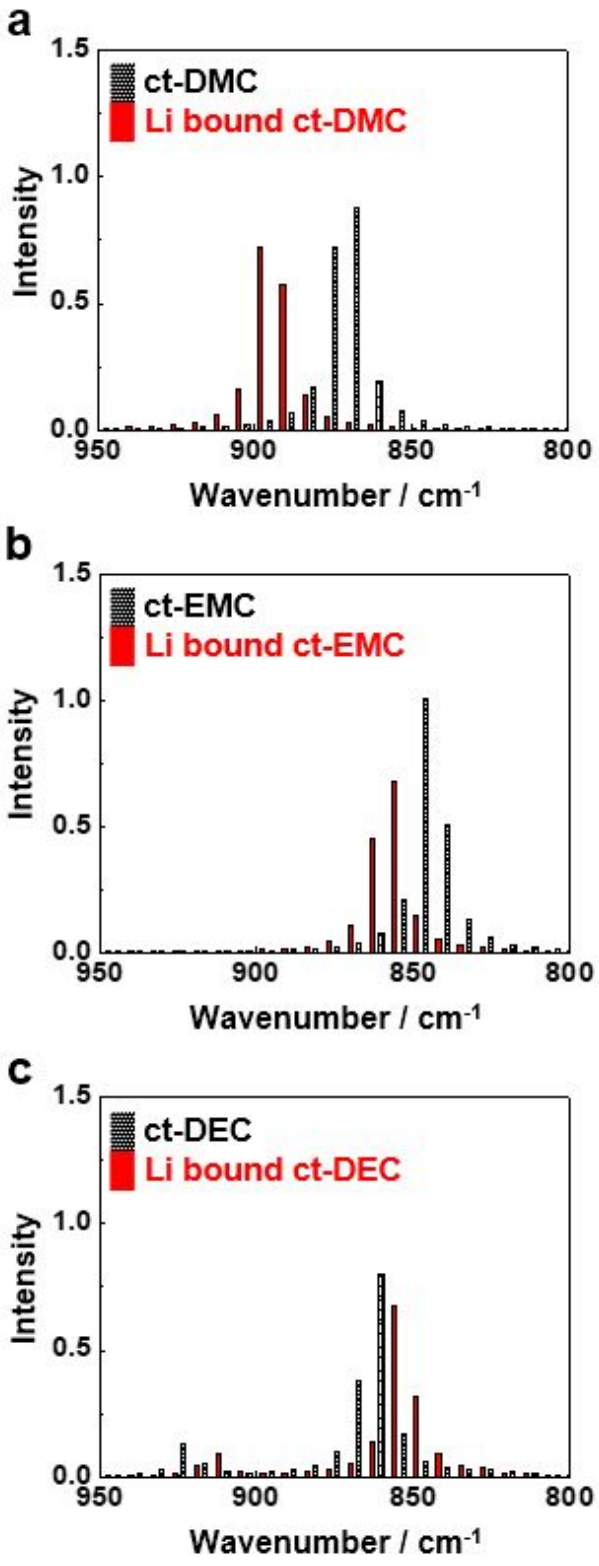

Figure S7. Calculated Raman spectra of ct- LCs (black) and Li bound ct-LCs (red) for (a) DMC, (b) EMC, and (c) DEC in the range of 950–800 cm^{-1}.

Determination of the coordination/solvation numbers by Raman spectroscopy

The coordination number of PF_6^- anion per Li ion (N_a) was determined from the relative Raman intensities of peak A and peak B (I_A and I_B, respectively).

$$N_a = I_B / (I_A + I_B) \quad (7)$$

In addition, the coordination numbers of cc and ct conformers per Li ion (i.e., solvation number), N_s, are defined as below.

$$N_s = [\text{Li-bound LC}] / [LiPF_6] \quad (8)$$

Multiple studies reported that the coordination number of the CIPs in DMC electrolytes is four, [10,11] which matches well with our own results. Lately, it was reported that in 9.6 mol% (~ 1 M) $LiPF_6$ DMC solution, $Li^+(\text{ct-DMC})_{1.1}(\text{cc-DMC})_{1.7}(PF_6^-)_{1.1}$ was determined using neutron diffraction measurements.[10] More recently, $Li^+(\text{ct-DMC})_{0.75}(\text{cc-DMC})_{2.25}ClO_4^-$ was deduced using DFT calculation.[11] These results are decently consistent with our Raman result (Figure S7). In $LiPF_6$-DMC and $LiPF_6$-EMC, the coordination number of PF_6^- anion per Li-ion is close to one (0.7–0.8). In addition, the total number of LC molecules coordinated to one Li ion (the solvation number) over 1–3 M concentration nears three: one ct-LC and two cc-LCs.

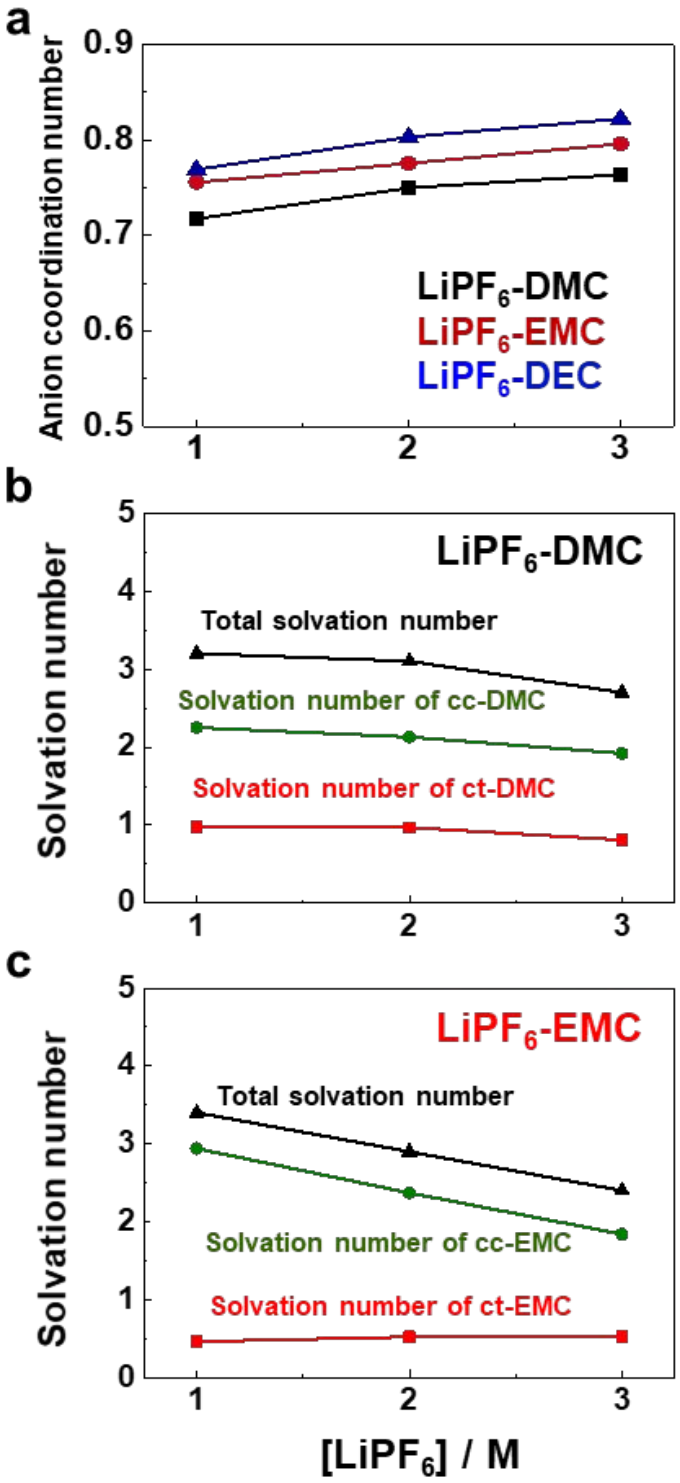

Figure S8. (a) Anion coordination number, (b and c) solvation numbers of total-LC, cc-LC, and ct-LC in (b) $LiPF_6$-DMC and (c) $LiPF_6$-EMC obtained from Raman measurements.

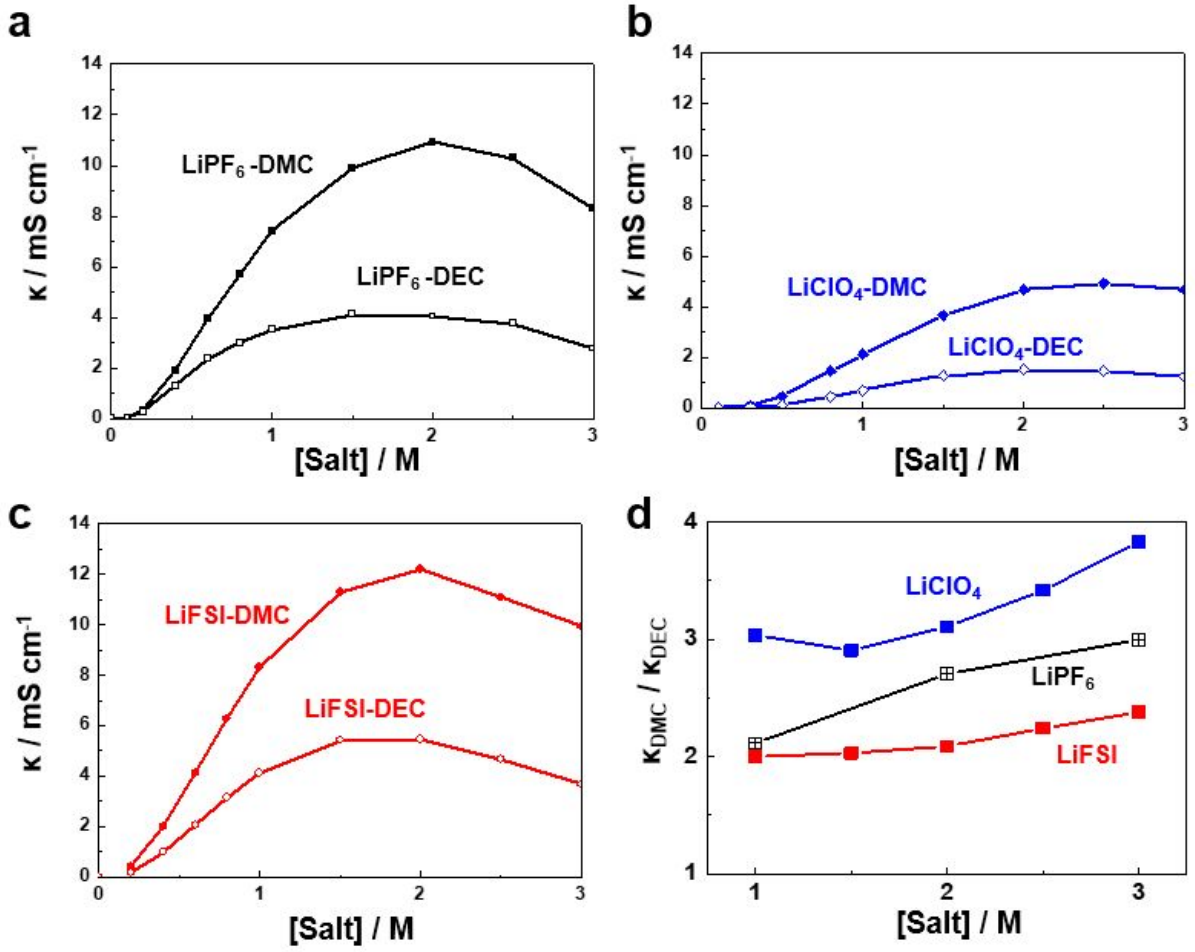

Figure S9. Ionic conductivities as a function of salt concentration of solutions: (a) $LiPF_6$-DMC, $LiPF_6$-DEC, (b) $LiClO_4$-DMC, $LiClO_4$-DEC, and (c) LiFSI-DMC and LiFSI-DEC. (d) Ionic conductivity ratios ($\kappa_{DMC}/\kappa_{DEC}$) of $LiPF_6$ $LiClO_4$ and LiFSI salt as a function of salt concentration at 25 °C.

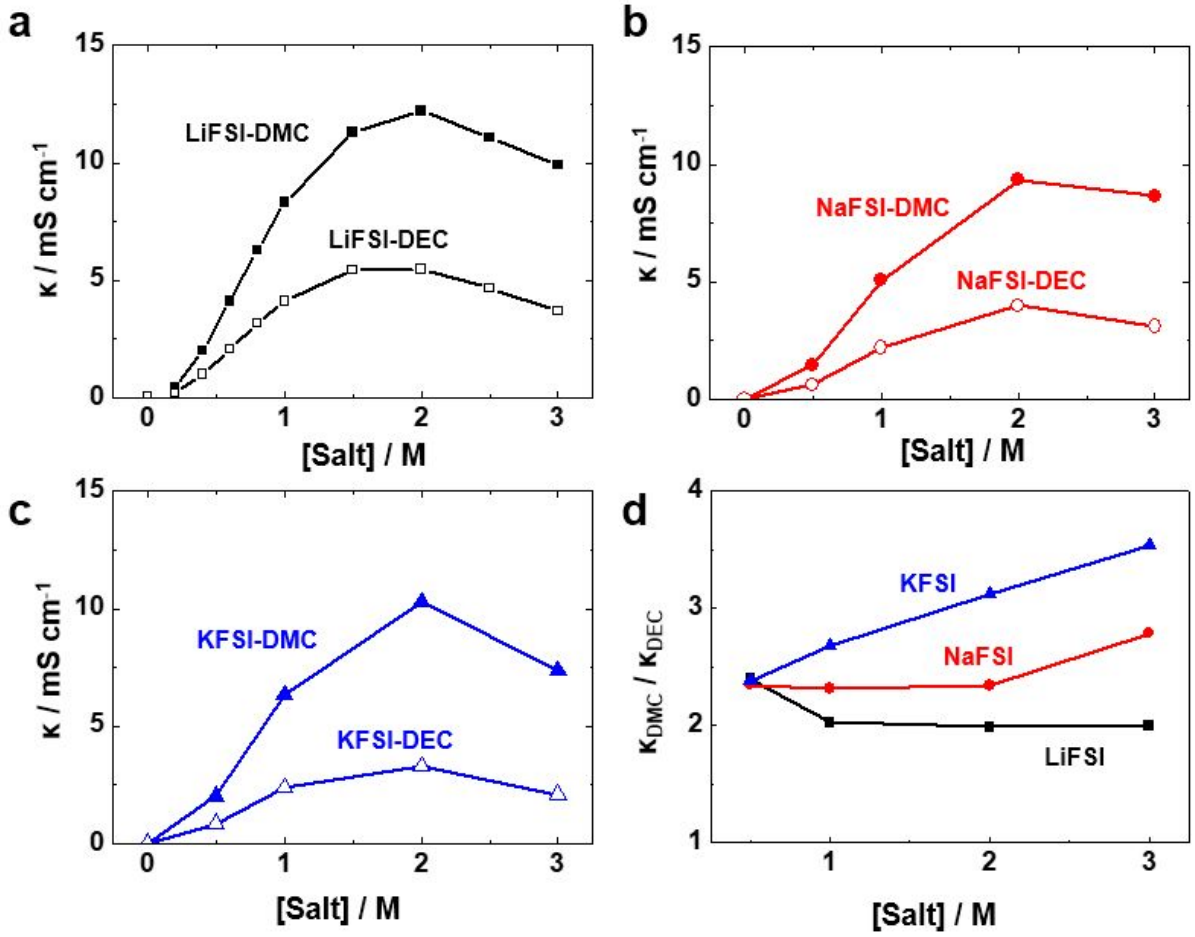

Figure S10. Ionic conductivities as a function of salt concentration of solutions: (a) LiFSI-DMC, LiFSI-DEC, (b) NaFSI-DMC, NaFSI-DEC, and (c) KFSI-DMC and KFSI-DEC. (d) Ionic conductivity ratios ($\kappa_{DMC}/\kappa_{DEC}$) of XFSI (X = Li, Na, and K) salt as a function of salt concentration at 25 °C.

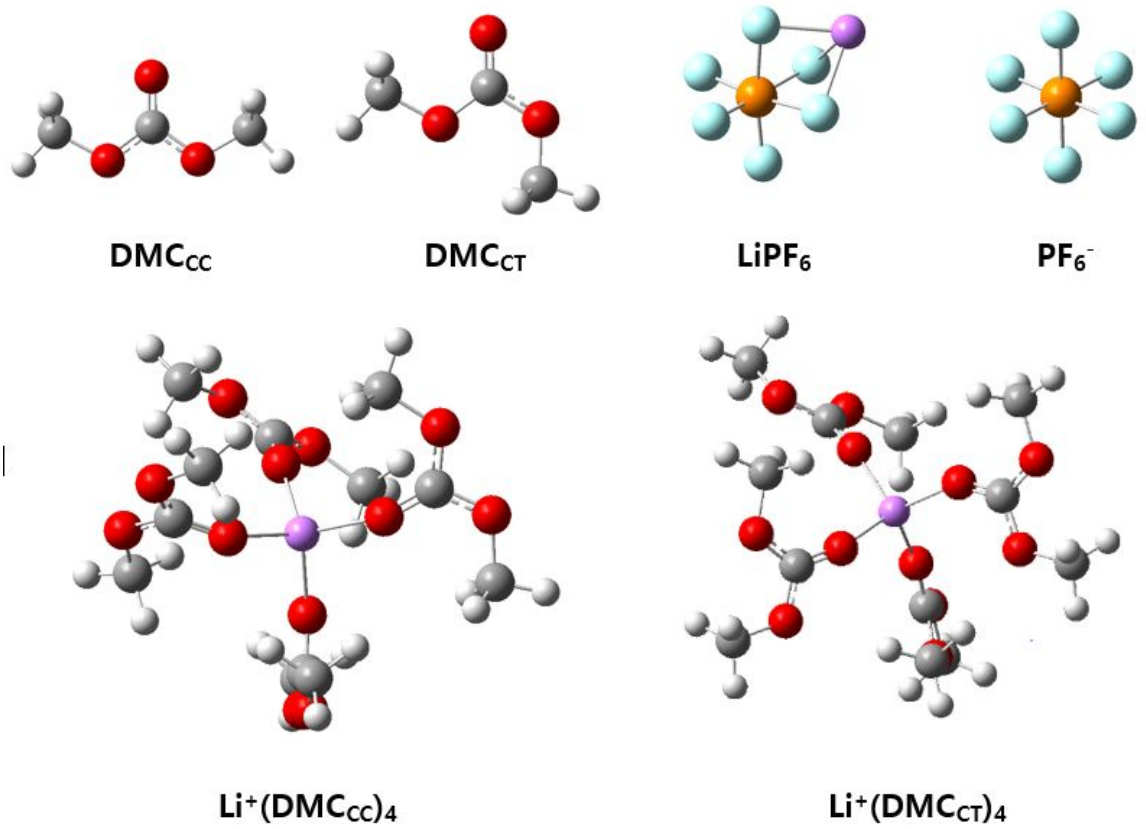

Figure S11. Optimized structures of DMC_{CC}, DMC_{CT}, $LiPF_6$, PF_6^-, $Li^+(DMC_{CC})_4$, and $Li^+(DMC_{CT})_4$.

(:Lithium, :Carbon, :Fluorine, :Hydrogen, :Oxygen, :Phosphorus)

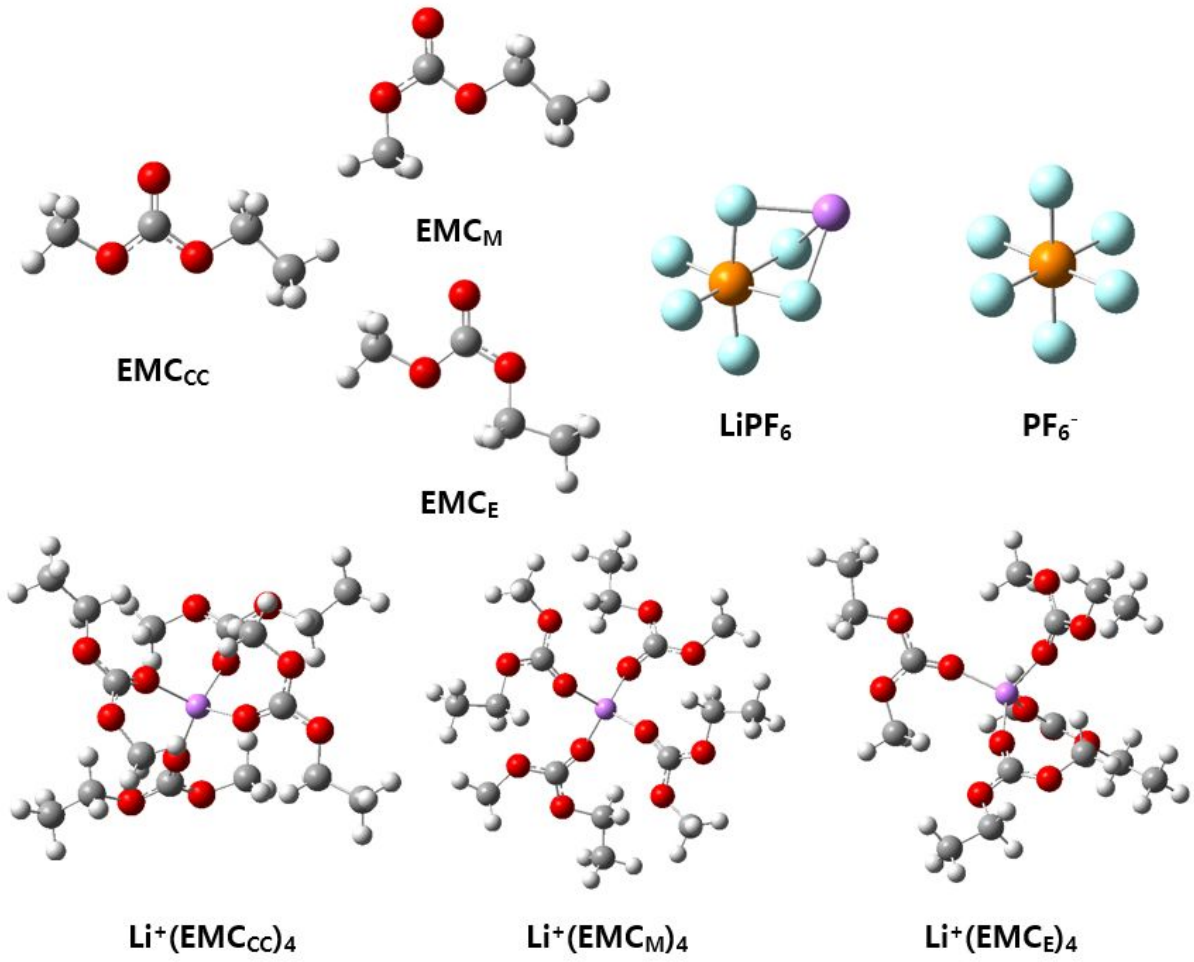

Figure S12. Optimized structures of EMC_{CC}, EMC_M, EMC_E, $LiPF_6$, PF_6^-, $Li^+(EMC_{CC})_4$, $Li^+(EMC_M)_4$ and $Li^+(EMC_E)_4$.

(:Lithium, :Carbon, :Fluorine, :Hydrogen, :Oxygen, :Phosphorus)

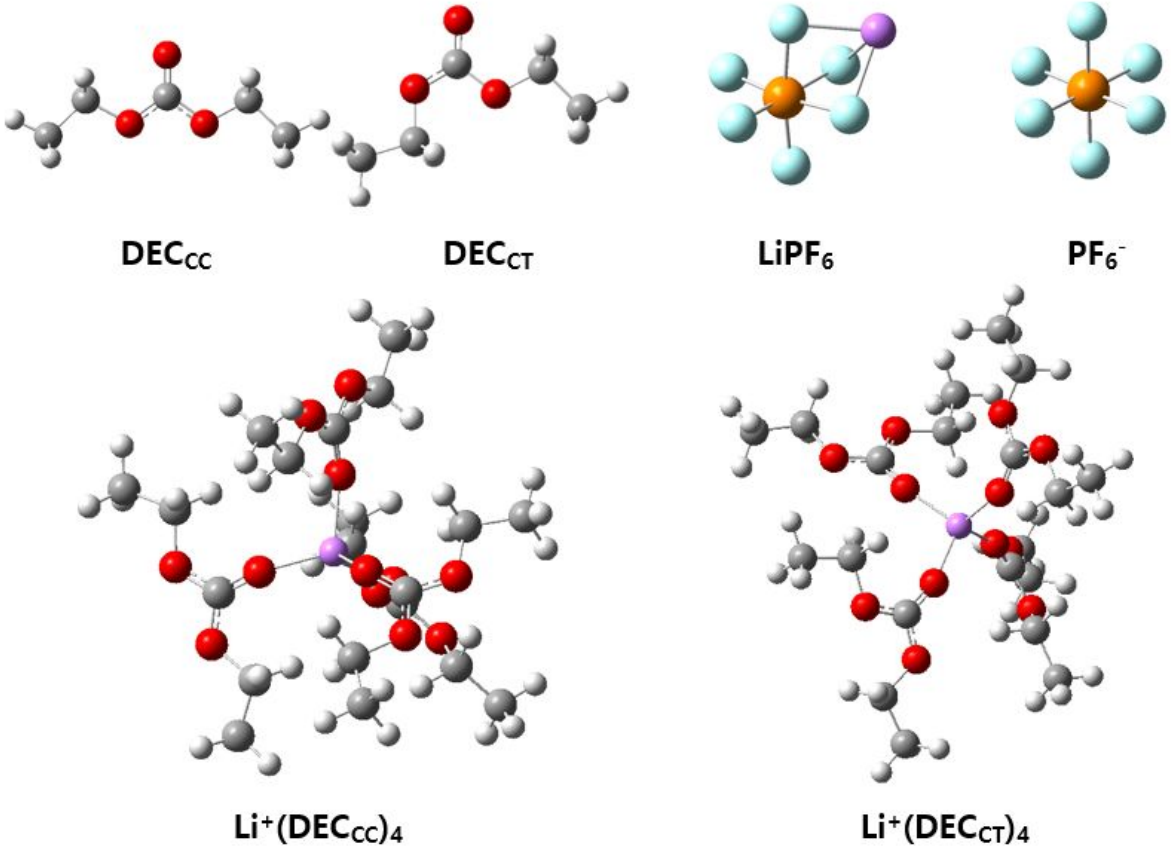

Figure S13. Optimization structures of DEC_{CC}, DEC_{CT}, $LiPF_6$, PF_6^-, $Li^+(DEC_{CC})_4$ and $Li^+(DEC_{CT})_4$.

(:Lithium, :Carbon, :Fluorine, :Hydrogen, :Oxygen, :Phosphorus)

References

(1) Buchner, R.; Hefter, G., Interactions and Dynamics in Electrolyte Solutions by Dielectric Spectroscopy. *Phys. Chem. Chem. Phys.* **2009**, *11*, 8984-8999.

(2) Eberspächer, P.; Wismeth, E.; Buchner, R.; Barthel, J., Ion Association of Alkaline and Alkaline-Earth Metal Perchlorates in Acetonitrile. *J. Mol. Liq.* **2006**, *129*, 3-12.

(3) Barthel, J.; Hetzenauer, H.; Buchner, R., Dielectric Relaxation of Aqueous Electrolyte Solutions. I. Solvent Relaxation of 1: 2, 2: 1, and 2: 2 Electrolyte Solutions. *Ber. Bunsenges. Phys. Chem.* **1992**, *96*, 988-997.

(4) Becke, A. D., Density-Functional Thermochemistry. III. The Role of Exact Exchange. *J. Chem. Phys.* **1993**, *98*, 5648−5652.

(5) Lee, C.; Yang, W.; Parr, R. G., Development of the Colle-Salvetti Correlation-Energy Formula into a Functional of the Electron Density. *Phys. Rev. B: Condens. Matter Mater. Phys.* **1988**, *37*, 785−789.

(6) Frisch, M. J.; Trucks, G. W.; Schlegel, H. B.; Scuseria, G. E.; Robb, M. A.; Cheeseman, J. R.; Scalmani, G.; Barone, V.; Mennucci, B.; Petersson, G. A., et al., *Gaussian 09u, Revision D.01; Gaussian*, Inc.: Wallingford, CT, **2009**.

(7) Bockris, J. O. M.; Conway, B. E.; White, R. E. *Modern Aspects of Electrochemistry 1: Ionics*; Springer Science & Business Media: Berlin, Germany, 2012.

(8) Kim, S. U.; Srinivasan, V., A Method for Estimating Transport Properties of Concentrated Electrolytes from Self-Diffusion Data. *J. Electrochem. Soc.* **2016**, *163*, A2977.

(9) Feng, Z.; Higa, K.; Han, K. S.; Srinivasan, V. Evaluating Transport Properties and Ionic Dissociation of Lipf6 in Concentrated Electrolyte. *J. Electrochem. Soc.* **2017**, *164*, A2434.

(10) Kameda, Y.; Saito, S.; Umebayashi, Y.; Fujii, K.; Amo, Y.; Usuki, T. Local Structure of Li^+ in Concentrated $LiPF_6$–Dimethyl Carbonate Solutions. *J. Mol. Liq.* **2016**, *217*, 17-22.

(11) Chapman, N.; Borodin, O.; Yoon, T.; Nguyen, C. C.; Lucht, B. L. Spectroscopic and Density Functional Theory Characterization of Common Lithium Salt Solvates in Carbonate Electrolytes for Lithium Batteries. *J. Phys. Chem. C* **2017**, *121*, 2135-2148.